Original Research Article

Using Shape Analysis of Liver Fat Droplet Morphology to Provide Quantitative Insights Into Staging of Nonalcoholic Fatty Liver Disease

Cinty Lin

Mountain View High School, 3535 Truman Avenue, Mountain View, CA 94040, United States

ABSTRACT

Nonalcoholic fatty liver disease (NAFLD; recently redefined as metabolic dysfunction-associated steatotic liver disease, MASLD) is one of the most common chronic liver diseases worldwide and is strongly associated with obesity, type 2 diabetes, metabolic syndrome, and insulin resistance. NAFLD is defined by the accumulation of fat in more than five percent of hepatocytes without excess alcohol use. Current staging systems categorize liver histology into discrete groups based on visual assessment, but subtle differences in fat droplet morphology are difficult for pathologists to detect. Precise histological staging is important for understanding disease severity. This study applies the Linearized Compressed Polar Coordinates (LCPC) Transform, a spatial algorithm, to quantify the pure shape of macrovesicular steatosis in NAFLD liver histology with the goal of identifying objective morphological subtypes of fat droplets. Shape analysis followed by Principal Component Analysis (PCA) and density-based clustering revealed at least three droplet groups that may represent previously uncharacterized morphological subtypes. These findings suggest that quantitative shape analysis could provide additional information that supports future efforts to refine NAFLD staging and improve diagnostic precision.

Keywords: Non-alcoholic fatty liver disease; metabolic dysfunction-associated steatotic liver disease; LCPC Transform; cell morphology

INTRODUCTION

Nonalcoholic fatty liver disease (NAFLD) is one of the most common chronic liver diseases worldwide and is strongly associated with obesity, type 2 diabetes, metabolic syndrome, and insulin resistance (1, 2). NAFLD is characterized by the abnormal presence of steatosis, or fat, exceeding 5% in the liver without excess alcohol intake (2, 3). The existing nomenclature of NAFLD was recently revised to metabolic dysfunction-associated steatotic liver disease (MASLD) by international consensus to reduce stigmatizing language, better reflect underlying disease mechanisms, and establish clearer diagnostic criteria (4). For clarity and consistency with prior studies and the source literature used, we retain the NAFLD/NASH terminology throughout the remainder of the manuscript. The histological spectrum of NAFLD begins from simple steatosis (fatty liver), nonalcoholic steatohepatitis (NASH), and later progresses to cirrhosis, and its final stage, hepatocellular carcinoma (HCC) (5). Histologically, NASH is characterized by excessive macrovesicular steatosis, lobular inflammation, and

Corresponding author: Cinty Lin, E-mail: cinty.lin.cinty@gmail.com.

Accepted January 21, 2026
https://doi.org/10.70251/HYJR2348.41422429

hepatocellular ballooning, with or without associated fibrosis (6). Currently, liver biopsies remain the gold standard for diagnosing NAFLD. Liver biopsies can distinguish between NASH and non-NASH cases, and one study found that early biopsy was associated with a higher proportion of patients ultimately presenting with milder disease, reduced progression to severe stages, and improved predicted survival (2). Currently, NASH is staged using these three scoring systems: the Brunt system, the NASH CRN system, and the SAF system (3). The Brunt and NASH CRN systems categorize severity from mild to severe based on steatosis, inflammation, and ballooning, while the SAF system quantifies disease activity as the sum of lobular inflammation and ballooning scores from 0–4 (3). While liver biopsy-based histological staging remains the gold standard for NASH diagnosis and differentiating it from other diseases, it has several limitations. Sampling error is a major concern because a biopsy represents a tiny fraction of the liver, and disease distribution is often uneven. Analyzing an insufficient or unrepresentative sample could skew accuracy, as the length and quality of the sample are crucial for evaluating key pathological features (7).

Recent advances in computational pathology have enabled automated histology image analysis in NAFLD. Machine learning is one of the many techniques computational biologists use to recognize patterns in medical images. Machine learning algorithms rely on labeled training medical data based on human knowledge on the data to learn and formulate predictions when fed with testing data (8). Traditionally, human experts relied on their medical knowledge for feature extraction, but deep learning eliminates the burden of manual feature engineering by discovering and learning hidden patterns with minimally preprocessed data, increasing the accessibility of machine learning techniques to all researchers (9). Biopsies can be analyzed like a pathologist through deep learning techniques like convolutional neural networks to classify features of NASH, such as fibrosis, ballooning, inflammation, and steatosis (10). However, a limitation of deep learning is that it is reliant on human-derived labels for it to know what is healthy versus affected. Due to the high cost of expert annotated images, medical datasets are often scarce, leading to models that may overfit to limited data and produce unreliable results (11). Furthermore, medical data is typically noisy, heterogeneous, and unclear, further challenging the model's ability to extract reliable, accurate features from the image (12). Therefore, if humans are unaware of unknown subtypes, then deep learning will not know they exist either. Thus, new methods for objectively identifying unknown subtypes are necessary if deep learning is to also identify them based on labeled training data, which is the goal of the present study.

Fat droplet morphology is known to vary but has not been quantitatively measured or analyzed. Furthermore, current staging uses broad features instead of quantitative shape metrics. The LCPC Transform, a novel spatial algorithm, has not been applied to NAFLD droplet morphology before. This research intends to determine whether LCPC-based shape analysis can identify objective morphological subtypes of fat droplets and possibly contribute to future refinements in NAFLD staging. The identification of unknown morphological subtypes will create deeper insights into the biology of fatty liver disease and will enhance diagnostics to predict clinical outcome.

METHODS AND MATERIALS

Image analysis and preprocessing steps were performed on NAFLD liver histology images collected by taking screenshots of histology images from journal articles (13-20). Fat droplets that did not have a clear border were not segmented, while ones that did have a clear border were included. After masks of each droplet were extracted, they were rotated and resized before applying the LCPC Transform technique; all via open-source Python programming scripts (21, 22). The LCPC Transform is a method used to objectively and quantitatively capture the complexities of any two-dimensional shape as a discrete sinusoid wave. In this case, we measure the pure shape of the biological feature. "Pure shape" refers to two objects being resized to the same dimensions, which removes the effect of size when comparing their shapes. Before resizing, cell contours must be oriented such that the longest internal line within each cell is identified. Each contour is then rotated such that this line becomes horizontal and also becomes the width of the contour. When resizing, the width of a contour is made to become 400-pixels wide. Also when resizing, it is important to constrain the aspect ratio to ensure the shape is not skewed during the process. This resizing process allows for comparison of the pure shape of two cells from different images, even if the magnification of each image were different. Thus, pure shape removes the effect of size on the shape.

The liver histology images were automatically segmented using Fiji, an open-source image processing

software, and manually pruned to ensure consistency among all segmented fat droplets. Masks were generated of the contours of each fat droplet in the image. The masks were manually spaced apart such that no contour is in contact with its neighbors. These spaced-out masks were then permanently flattened onto a white canvas. This allowed for a Python script to isolate each cell contour as a separate object on its own white canvas.

For each composite mask, the following protocol is applied before the radial grid LCPC processing step. Each step is performed via an open-source Python script (21). Steps 7-9 are responsible for extracting pure shape.

1. Magnify the composite mask image by 3 times (this avoids small cells being too tiny for analysis)
2. Isolate each object (fat droplet) onto its own white canvas
3. Thicken the lines twice to prevent it from being eroded in the future steps
4. Trim the margin of the image to 1 pixel
5. Add 100 pixels to the margins
6. Rotate the image such that its longest internal length is horizontal
7. Trim the margin of the image back to 1 pixel
8. Resize width to 400 pixels while constraining aspect ratio
9. Add 100 pixels to the margins
10. Rotate the image 90 degrees clockwise

When using the LCPC Transform, the desired biological feature is segmented from the original image and overlaid with a radial or parallel grid system. In this case, the radial grid system was used because each fat droplet is a closed circular shape, making this grid system an optimal choice. First, a mask of the outline for each segmented fat droplet was created and the center of the smallest bounding box around the shape is found for each shape. Then, a 360-degree radial grid, whose origin is the center of the bounding box, is spaced evenly every 5 degrees and is overlaid on the fat droplet, producing a dot plot of 71 points that are a stencil of the original image. The distances between the origin and the intersection of each radial line with the edge of the shape is calculated. If multiple intersections lie on the same radial line, they are summed into one value for that radial position. This results in a discrete sinusoid wave that represents the shape's contour. The resulting sinusoidal wave is then processed with the Fast Fourier Transform (FFT) to obtain a multidimensional representation of the shape, which outputs a range of frequencies that represent the spatial complexity of the feature of interest (23). All of the shapes' FFT results are compiled into a single data frame that will be used for the final step.

Median standardization is used to standardize the compiled FFT data before performing Principal Component Analysis (PCA) because the results from the LCPC scripts inherently contain outliers. PCA is performed to identify the top three principal components to help with visualizing and identifying unique subgroups of fat droplets within the high-dimensionality data. To statistically validate the visually identified morphological groups, the first round of DBSCAN (Density-Based Spatial Clustering Of Applications With Noise) was applied to the full PCA dataset, while a second round was applied to the subset of points labeled as noise in the first round. The first round used an epsilon value of 0.4 and min_samples of 10; the second round used an epsilon of 0.9 and min_samples of 4. Cluster quality in each round was assessed using silhouette scores. All analyses (PCA, DBSCAN, silhouette score) were performed using Python's Scikit-learn library.

RESULTS

The analysis assessed segmented fat droplets from liver histology images. After applying the LCPC Transform and compiling the FFT data, PCA was done to visualize morphological variation, followed by DBSCAN and silhouette score analysis to evaluate potential groupings. The results below summarize the dataset and the features observed through these analyses.

Dataset Description

A total of 28 screenshots were collected from various papers (13-20). Eight were omitted because of poor resolution, unclear steatosis formation, or the absence of visible fat droplets. From the remaining 20 images, 1,650 fat droplets were segmented. The droplets ranged from circular to slightly elliptical, but also appeared as smooth to mildly jagged closed contours.

PCA and Cluster Identification

PCA was performed on the median-standardized FFT dataset. A 3D PCA plot using the first three principal components is shown in Figure 1. The distribution of points reveals several potential visually distinct clusters.

By rotating the plot and viewing it from multiple angles, four morphological groupings appear to be present based on point density and separation (Figure 2). These views include PC1 vs PC2 and PC2 vs PC3

perspectives.

To illustrate how the PCA clusters relate to actual droplet shapes, several droplets were labeled according to their PCA coordinates. Since only pure shape was measured, the height of all droplets is approximately equal. Examples for Groups 1 and 2, along with nearby outliers, are shown in Figure 3. Examples for Groups 3 and 4 are shown in Figure 4. A magnified view of the Group 1 graph is shown in Figure 5 with labeled fat droplets in that zoomed region.

These groups result from exploratory visual analysis and require statistical validation. To provide quantitative support, DBSCAN and silhouette scores were applied. The primary round of DBSCAN identified two dense clusters and a set of outliers (green, red, and purple points in Figure 6A). Examination of fat droplets associated with the visually determined groups (Groups 3 and 4 in Figure 4) revealed subtle phenotypic differences within

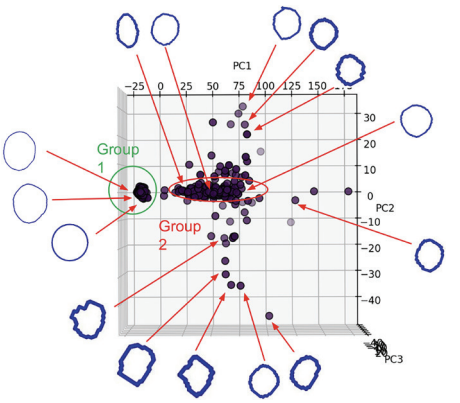

Figure 3. *Examples of fat droplets associated with Group 1, Group 2, and nearby outliers based on PC1 and PC2 values. Each group labeled in the graphs was identified by visual approximation of overlapping points. The difference in thickness of the shapes has no effect on these results.*

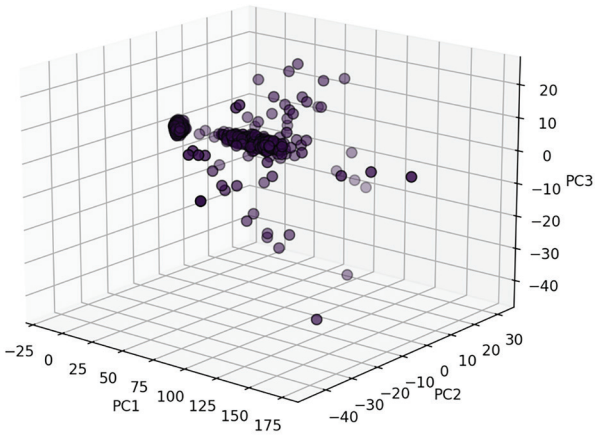

Figure 1. *Three-dimensional PCA plot using the first three principal components.*

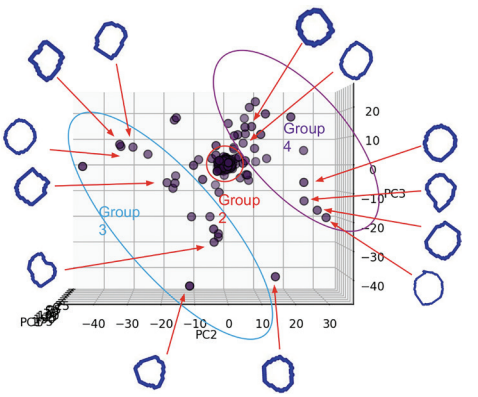

Figure 4. *Examples of fat droplets associated with Group 3, Group 4, and nearby outliers based on PC2 and PC3 values. Each group labeled in the graphs was identified by visual approximation of overlapping points. The difference in thickness of the shapes has no effect on these results.*

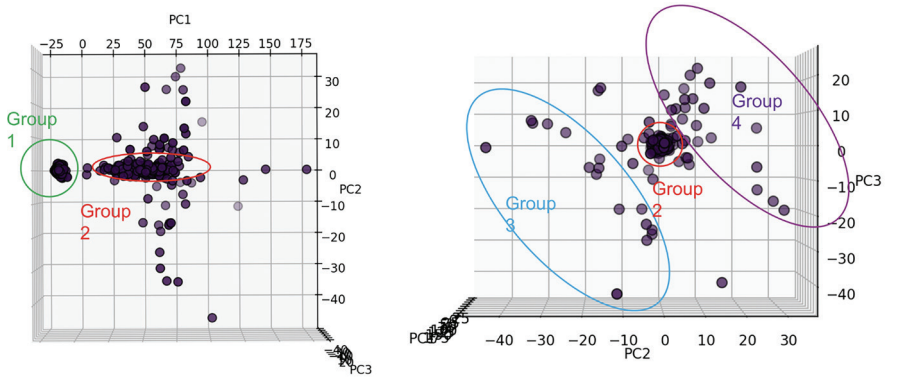

Figure 2. *PCA plots viewed from different orientations showing four potential visually distinct groupings. Group labels were assigned based on visual inspection.*

the outlier group, prompting a secondary DBSCAN analysis. The primary clusters exhibited a silhouette score of 0.803, indicating they are well-defined and compact. The two clusters identified in the noise group from the first round showed a weaker silhouette score of 0.353, likely due to limited sample size. To reflect this uncertainty, a question mark was appended to the labels "Group 3A" and "Group 3B". However, the second round of DBSCAN did not stratify the green cluster in Figure 6A into two dense, well-separated groups, as initially hypothesized based on the phenotypic differences observed in Figure 4. Therefore, we can only define a single Group 3, which is shown as the gray cluster in Figure 6B.

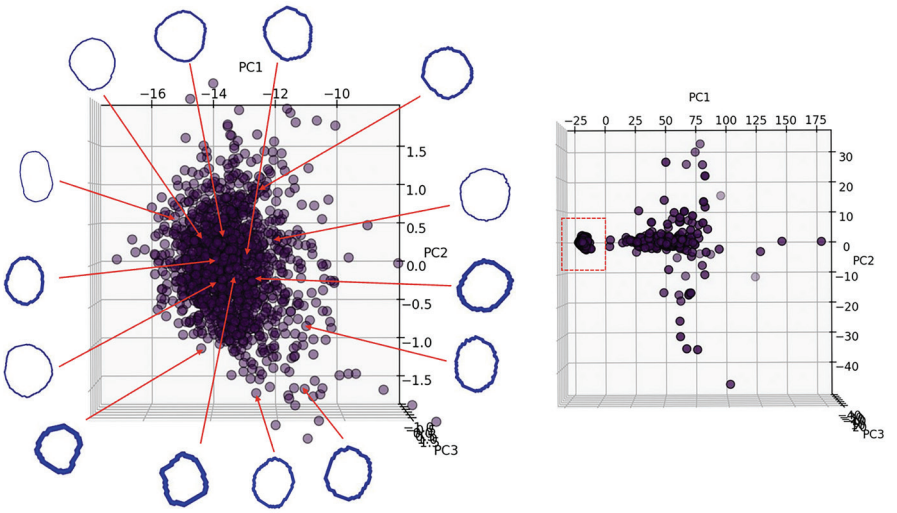

Figure 5. *A zoomed-in view of the principal component space for the densely populated Group 1 cluster (red dotted line). Further examples of fat droplets associated with Group 1 are presented. The difference in thickness of the shapes has no effect on these results.*

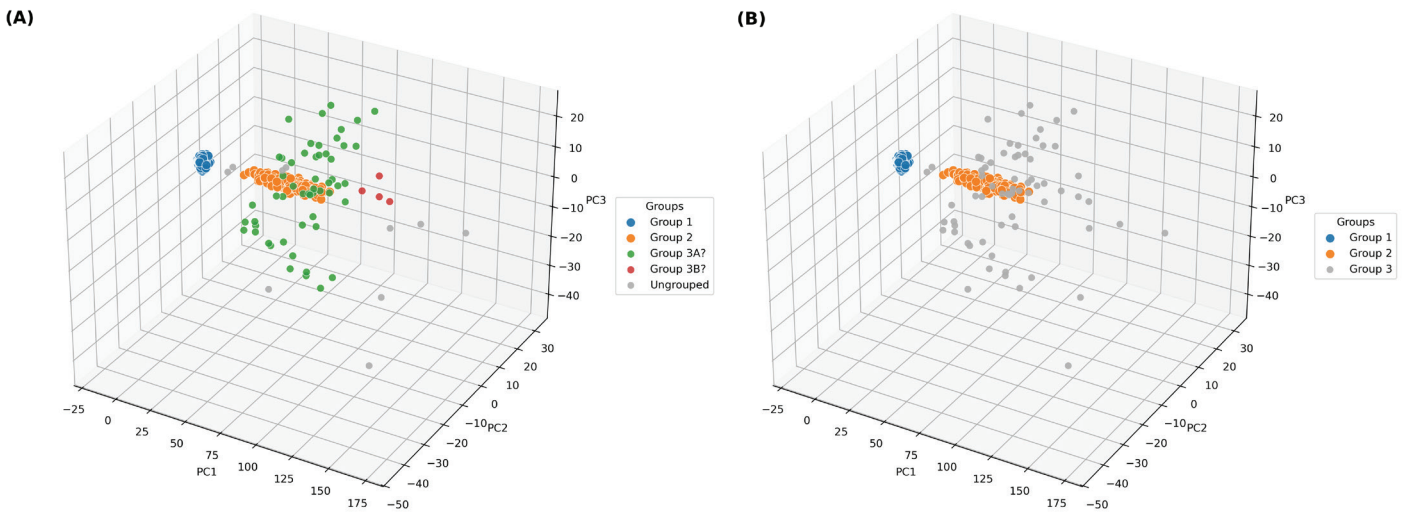

Figure 6. *(A) Three-dimensional PCA plot showing color-coded clusters identified through two consecutive rounds of DBSCAN analysis. Although qualitative evidence suggested the possible presence of two subgroups within Group 3, the second round of DBSCAN did not provide sufficient quantitative support for separating these into distinct clusters. (B) PCA plot in which the tentative Group 3A?, Group 3B?, and noise points from (A) are consolidated into a single Group 3.*

DISCUSSION

PCA revealed multiple morphological groupings, indicating that fat droplets vary in ways that can be objectively and quantitatively stratified. Each group in Figure 3 and 4 exhibits subtle shape features that distinguish them from other groups. Without the LCPC Transform, the naked eye is unable to objectively identify the themes that represent these groups. These morphological differences primarily involve variations in aspect ratio (roundness vs. ellipticity), boundary smoothness/irregularity, and asymmetry. Such differences are not captured by traditional NAFLD staging, which relies on broad histological categories rather than finer quantitative patterns. The presence of multiple distinct shape types may suggest that steatosis involves intermediate morphological states. However, any claims regarding progression through intermediate morphologies are speculative, as the images originate from heterogeneous sources and represent multiple disease stages. Accordingly, these interpretations should be viewed as hypotheses that require future validation using comprehensive, stage-controlled datasets derived from consistent sources.

Implications of Morphological Subtypes for NAFLD Progression and Grading

The presence of morphological subtypes is consistent with the idea that NAFLD may progress along a continuum rather than through rigid, discrete stages. There are at least three clusters, with the third group potentially being two based on visual inspection of the phenotypes due to statistical uncertainty. To illustrate differences between subtypes, visual analogies are used. Group 1 droplets are highly rounded and bead-like, similar to marbles, whereas Group 2 droplets are slightly elongated, resembling river pebbles. Group 3A shows irregular, asymmetric forms analogous to uneven clay fragments, and Group 3B consists of irregularly rounded beads with contours similar to small ponds on a map. These analogies are intended for visualization, not strict classification. These analogies are intended only for illustration rather than strict classifications and to better understand how the shapes differ. Based on the observation that fat droplets in adipocytes are round and smooth (24), one could hypothesize that earlier steatosis could begin with more regular and symmetric droplets before progressing to abnormal phenotypes; alternatively, that abnormal shapes are a subtype of progression.

The detail visible in the most compact cluster (Group 1, shown in Figure 5) further reinforces the power of this quantitative approach, because normal adipocytes are round in shape. Figure 5, which focuses on the droplets with roughly smooth shapes, reveals that within this visually homogenous group, there exists quantitative variations in the shape that can be objectively measured by the LCPC Transform.

Quantifying lipid droplet shape could help visualize how droplets change from irregular to more rounded forms, or vice versa, as steatosis develops. Identifying these intermediate patterns may inform the development of a more refined grading system that better captures biological variation in steatosis. Patient-level clinical variables could not be tracked along with the images because in the original publications these were representative of typical NAFLD cases.

Despite this, shape-based metrics may serve as a complementary biomarker for automated NAFLD grading. AI models often overlook subtle structural details when relying solely on raw images, because if human experts cannot reliably identify these differences, AI systems are unlikely to do so either. Incorporating quantitative measurements from the LCPC Transform has the potential to improve model performance and reduce subjectivity in steatosis assessment, although further clinical validation will be required to establish clinical utility.

CONCLUSION

The purpose of this study was to determine whether shape analysis using the LCPC Transform can provide objective and quantitative evidence of morphological subtypes of macrovesicular steatosis in NAFLD liver histology. Current NAFLD staging relies on a pathologist's visual interpretation of common histological items: hepatocyte ballooning and Mallory-Denk bodies, lobular inflammation, portal inflammation, steatosis, and fibrosis (25). Although these features capture the general progression from steatosis to NASH, cirrhosis, or HCC, the human eye cannot reliably identify or quantify subtle structural differences among individual fat droplets. In a study evaluating the intrarater and interrater reliability of histologic NAFLD features, hepatocyte ballooning and fibrosis bodies were found to be the most reliable and showed the strongest correlation with disease activity (25). In contrast, while steatosis items demonstrated moderate reliability, they show negligible correlation with overall disease activity, highlighting a key feature of the histological assessment system (25). By measuring pure shape and applying PCA to the LCPC output, this

study identified at least three groups of fat droplets that may represent intermediate or transitional morphological states within the broader continuum of NAFLD. These findings suggest that quantitative morphology has the potential to complement existing histological staging.

There are several limitations to consider. Publicly available liver histology datasets are limited, and many of the images used here were obtained via screenshots, reducing the number of usable samples and introducing variability in resolution, selection, and representativeness. As a preliminary pilot study, the purpose of this work is to demonstrate the promise of the LCPC Transform method; further validation with larger, high-quality, stage-controlled datasets is required to confirm reproducibility and generalizability. Although many droplets were segmented per image, a larger and more diverse dataset would strengthen the reliability of the findings. Manual and Fiji based segmentation also risks minor inaccuracies that may slightly distort the true outline of each droplet. Such errors could influence the LCPC measurements and affect the placement of droplets in PCA space.

Future work should focus on building a larger, higher resolution image dataset, ideally sourced directly from laboratory-collected histology slides. Automated segmentation pipelines, such as those described by Esparza *et al*., could help reduce segmentation errors and ensure consistency across samples. Their work showed that quantitative morphological features correlate with steatosis severity but required further validation of clinical relevance (26). Expanding on this direction by applying the LCPC Transform could provide the needed foundation to interpret the biological and diagnostic significance of these shape-based subtypes. Additionally, future work should integrate patient-level clinical variables to assess whether lipid droplet morphology quantified by the LCPC Transform correlates with clinically relevant disease characteristics.

Overall, quantitative shape data generated through the LCPC Transform may give pathologists and liver researchers a new tool for discovering previously unrecognized subtypes of lipid droplets. With further validation, these features could help refine NAFLD staging, improve diagnostic accuracy, and guide more tailored clinical decision making.

ACKNOWLEDGEMENTS

The author would like to thank Dr. David H. Nguyen, PhD, inventor of the LCPC Transform and Principal Investigator at the Tissue Spatial Geometrics Laboratory. This work would not have happened without inspiration from Dr. Nguyen to apply the LCPC Transform to liver histology images.

CONFLICT OF INTEREST

The author declares that there are no conflicts of interest related to this work.

REFERENCES

1. Riazi K, Azhari H, Charette JH, Underwood FE, King JA, Afshar EE, *et al*. The prevalence and incidence of NAFLD worldwide: a systematic review and meta-analysis. *Lancet Gastroenterol Hepatol*. 2022; 7 (9): 851-61. https://doi.org/10.1016/S2468-1253(22)00165-0
2. Nalbantoglu I, Brunt EM. Role of liver biopsy in nonalcoholic fatty liver disease. *World journal of gastroenterology: WJG*. 2014 Jul 21; 20 (27): 9026. https://doi.org/10.3748/wjg.v20.i26.8351
3. Kleiner DE, Makhlouf HR. Histology of NAFLD and NASH in adults and children. *Clinics in liver disease*. 2015 Dec 28; 20 (2): 293. https://doi.org/10.1016/j.cld.2015.10.011
4. Rinella ME, Sookoian S. From NAFLD to MASLD: updated naming and diagnosis criteria for fatty liver disease. *Journal of lipid research*. 2024 Jan 1; 65 (1). https://doi.org/10.1016/j.jlr.2023.100485
5. Hashimoto E, Taniai M, Tokushige K. Characteristics and diagnosis of NAFLD/NASH. *Journal of gastroenterology and hepatology*. 2013 Dec; 28: 64-70. https://doi.org/10.1111/jgh.12271
6. Santos JPM, Maio MC, Lemes MA, Laurindo LF, Haber JFS, Bechara MD, *et al*. Non-alcoholic steatohepatitis (NASH) and organokines: what is now and what will be in the future. *Int J Mol Sci*. 2022; 23 (1): 498. https://doi.org/10.3390/ijms23010498
7. Sumida Y, Nakajima A, Itoh Y. Limitations of liver biopsy and non-invasive diagnostic tests for the diagnosis of nonalcoholic fatty liver disease/nonalcoholic steatohepatitis. *World J Gastroenterol*. 2014; 20 (2): 475. https://doi.org/10.3748/wjg.v20.i2.475
8. Erickson BJ, Korfiatis P, Akkus Z, Kline TL. Machine learning for medical imaging. *Radiographics*. 2017; 37 (2): 505-15. https://doi.org/10.1148/rg.2017160130
9. Shen D, Wu G, Suk HI. Deep learning in medical image analysis. *Annu Rev Biomed Eng*. 2017; 19 (1): 221-48. https://doi.org/10.1146/annurev-bioeng-071516-044442
10. Heinemann F, Gross P, Zeveleva S, *et al*. Deep learning-based quantification of NAFLD/NASH

progression in human liver biopsies. *Sci Rep*. 2022; 12 (1): 19236. https://doi.org/10.1038/s41598-022-23905-3

11. Dhar T, Dey N, Borra S, Sherratt RS. Challenges of deep learning in medical image analysis-improving explainability and trust. *IEEE Transactions on Technology and Society.* 2023 Jan 4; 4 (1): 68-75. https://doi.org/10.1109/TTS.2023.3234203
12. Miotto R, Wang F, Wang S, Jiang X, Dudley JT. Deep learning for healthcare: review, opportunities and challenges. *Briefings in bioinformatics*. 2018 Nov; 19 (6): 1236-46. https://doi.org/10.1093/bib/bbx044
13. Băloşeanu CL, Streba CT, Vere CC, Comănescu VI, Rogoveanu I. Association between liver histology, carotid ultrasonography and retinal vascular changes in patients with nonalcoholic fatty liver disease (NAFLD). *Rom J Morphol Embryol*. 2012 Jan 1; 53 (3): 609-14.
14. Bantaloukas-Arjmand A, Giannakeas N. Fat Quantitation in Liver Biopsies Using a Pretrained Classification Based System. *Engineering, Technology & Applied Science Research.* 2018 Dec 1; 8 (6). https://doi.org/10.48084/etasr.2274
15. Cabezas J, Mayorga M, Crespo J. Nonalcoholic Fatty Liver Disease: A Pathological View. Liver Biopsy - Indications, Procedures, Results. InTech; 2012. doi: 10.5772/52622. https://doi.org/10.5772/52622
16. Chaim FD, Pascoal LB, Chaim FH, Palma BB, Damázio TA, da Costa LB, *et al*. Histological grading evaluation of non-alcoholic fatty liver disease after bariatric surgery: a retrospective and longitudinal observational cohort study. *Scientific Reports*. 2020 May 22; 10 (1). https://doi.org/10.1038/s41598-020-65556-2
17. Chan AW. Pathology of Non-Alcoholic Fatty Liver Disease. Topical Update - The Hong Kong College of Pathologists. 2015 January; 10 (1).
18. El-Kader SM. Non-alcoholic fatty liver disease: The diagnosis and management. *World Journal of Hepatology.* 2015; 7 (6): 846. doi: 10.4254/wjh.v7.i6.846.
19. Loomba R, Friedman SL, Shulman GI. Mechanisms and disease consequences of nonalcoholic fatty liver disease. *Cell.* 2021 May 13; 184 (10): 2537-64. doi: 10.1016/j.cell.2021.04.015.
20. Ntandja Wandji LC, Gnemmi V, Mathurin P, Louvet A. Combined alcoholic and non-alcoholic steatohepatitis. *JHEP Reports*. 2020 Jun 1; 2 (3): 100101. doi: 10.1016/j.jhepr.2020.100101.
21. Nguyen D. Pre-Processing-Tools-for-LCPC-Transform [Internet]. GitHub; 2025 May [cited 2025 Nov 29]. Available from: https://github.com/dh2nguyen/Pre-Processing-Tools-for-LCPC-Transform
22. Nguyen D. Radial-Grid-LCPC-Transform [Internet]. GitHub; 2025 May [cited 2025 Nov 29]. Available from: https://github.com/dh2nguyen/Radial-Grid-LCPC-Transform
23. Nguyen D. Translating the architectural complexity of the colon or polyp into a sinusoid wave for classification via the fast Fourier transform [Preprint]. arXiv:1801.06752 [Preprint]. 2018 Jan 21. Available from: https://arxiv.org/abs/1801.06752.
24. Fujimoto T, Parton RG. Not just fat: the structure and function of the lipid droplet. *Cold Spring Harb Perspect Biol.* 2011 Mar 1; 3 (3): a004838. doi: 10.1101/cshperspect.a004838.
25. Pai RK, Jairath V, Hogan M, Zou G, Adeyi OA, Anstee QM, Aqel BA, Behling C, Carey EJ, Clouston AD, Corey K. Reliability of histologic assessment for NAFLD and development of an expanded NAFLD activity score. *Hepatology*. 2022 Oct; 76 (4): 1150-63. https://doi.org/10.1002/hep.32475
26. Esparza J, Shrestha U, Kleiner DE, Crawford JM, Vanatta J, Satapathy S, *et al*. Automated segmentation and morphological characterization of hepatic steatosis and correlation with histopathology. *J Clin Exp Hepatol*. 2023; 13 (3): 468-78. https://doi.org/10.1016/j.jceh.2022.12.003